The Structure and Stability of the Disulfide-Linked γS-Crystallin Dimer Provide Insight into Oxidation Products Associated with Lens Cataract Formation

David C. Thorn†, Aidan B. Grosas†, Peter D. Mabbitt, Nicholas J. Ray, Colin J. Jackson and John A. Carver

Research School of Chemistry, *The Australian National University, Acton, ACT 2601, Australia*

Correspondence to John A. Carver: *john.carver@anu.edu.au*
https://doi.org/10.1016/j.jmb.2018.12.005
Edited by Sheena Radford

Abstract

The reducing environment in the eye lens diminishes with age, leading to significant oxidative stress. Oxidation of lens crystallin proteins is the major contributor to their destabilization and deleterious aggregation that scatters visible light, obscures vision, and ultimately leads to cataract. However, the molecular basis for oxidation-induced aggregation is unknown. Using X-ray crystallography and small-angle X-ray scattering, we describe the structure of a disulfide-linked dimer of human γS-crystallin that was obtained via oxidation of C24. The γS-crystallin dimer is stable at glutathione concentrations comparable to those in aged and cataractous lenses. Moreover, dimerization of γS-crystallin significantly increases the protein's propensity to form large insoluble aggregates owing to non-cooperative domain unfolding, as is observed in crystallin variants associated with early-onset cataract. These findings provide insight into how oxidative modification of crystallins contributes to cataract and imply that early-onset and age-related forms of the disease share comparable development pathways.

Introduction

The eye lens contains a high concentration of crystallin proteins arranged in a well-ordered, short-range array that allows for lens transparency and the refraction of light onto the retina, thus ensuring proper vision [1–3]. In mammals, the crystallins comprise three types (α, β, and γ), of which there are several isoforms. The α-crystallins are members of the small heat-shock protein family, whereas the β- and γ-crystallins are a structurally homologous superfamily of proteins that are not related to small heat-shock proteins [4–6]. β- and γ-crystallins have a monomeric mass of approximately 20 kDa and consist of two domains, each containing two Greek-key β-sheet motifs, which are adjoined by a short linking peptide [6–9].

There is little protein turnover in the eye lens, and thus, the crystallins are long-lived proteins that must maintain their structural integrity throughout life to preserve lens transparency [10–12]. Cataract occurs due to a loss of crystallin protein stability and the subsequent propensity of crystallins to partially unfold, leading to aggregation and precipitation [6,13]. While cataract acquired during early life commonly stems from destabilizing, inheritable mutations in crystallin proteins, age-related cataract is thought to originate from cumulative post-translational modifications (PTMs) [14,15]. Oxidation is a prevalent crystallin PTM in both aged and cataractous lenses [16,17] that increases the aggregation propensity of some crystallins *in vitro* [18–20]. Cysteine residues are the principal site of protein oxidation [16,21], and disulfide-linked crystallins are a major component of the insoluble fraction of cataractous lenses [22,23]. The key factor in preventing crystallin oxidation is the cellular reductant glutathione, the levels of which diminish with age, to the extent that it is severely depleted in cataractous lenses [24–26].

γS-crystallin (γS) is one of the major crystallins in the human lens [27], and its abundance increases with age due to postnatal expression [28]. Human γS in cataractous lenses is oxidized at specific cysteine residues [17], including *S*-methylation [29], *S*-glutathionylation [30], and intermolecular disulfide bond formation [23]. Indeed, γS forms disulfide-

linked dimers *in vitro* [31]. Disulfide-linked dimerization similarly occurs for the R14C mutant of γD-crystallin, leading to increased aggregation propensity and hereditary juvenile-onset cataract [32]. In light of this and the enhanced oxidative conditions in the aging lens, a detailed understanding of the structural and physiological implications of disulfide-linked dimerization of wild-type γS is needed. Herein, we isolated disulfide-linked, dimeric human γS and determined its structure by X-ray crystallography and small-angle X-ray scattering (SAXS). The significance of the disulfide bonding arrangement of the three clustered cysteine residues at positions 22, 24, and 26 is discussed. Furthermore, we provide biophysical and biochemical evidence for the role of the γS dimer in age-related cataract and the potential molecular mechanisms underlying this role.

Results

Structure of human γS disulfide-linked dimer

Human γS monomer was expressed heterologously in *Escherichia coli* and purified using anion-exchange and size-exclusion chromatography (SEC). Previously, γS was reported to undergo time-dependent dimer formation under ambient, oxidative conditions at slightly elevated pH, for example, pH 8 [31]. In the present study, γS monomer was readily converted to dimer at physiological pH (i.e., pH 7) by concentrating the monomer to a minimum of 20 mg mL^{-1} and leaving the protein at 4 °C for 1 week. Monomeric and dimeric forms of γS were isolated and checked for homogeneity and correct mass using SEC coupled to multi-angle light scattering (Fig. S1a).

The γS dimer was crystallized and its structure determined by X-ray crystallography to a resolution of 2.1 Å (Table 1). The crystal structure shows the canonical two-domain Greek-key motif β-strand arrangement for each monomeric subunit (Fig. 1a, top). The asymmetric unit consists of a dimer of γS arranged in the same orientation as is observed for the crystal structure of truncated βB1-crystallin [34] and the solution structure of full-length βB2-crystallin [35], which has been previously described as a QR configuration [36]. There are three cysteine residues in a loop close to the N-terminus of γS: C22, C24, C26. In each monomer in the asymmetric unit, the loop is cyclized by one intramolecular disulfide bond between C22 and C26 in each subunit (Fig. 1a, bottom, c and d). No other disulfide bonds were present in the crystallographic dimer observed in the asymmetric unit. However, electrospray ionization mass spectrometry (MS) of the γS dimer indicated the presence of three disulfide bonds, that is, a loss of 6 Da from the expected mass of two monomers (Fig. S1b). Inspection of symmetry mates within the crystal lattice revealed an alternative dimer interface having a C24:C24' disulfide bond as its principal intermolecular contact. Analysis of the dimer interface using PISA [37] indicated that this alternative interface buries 648 $Å^2$ of protein surface area. In addition to the intermolecular disulfide bond, there are several non-covalent intermolecular interactions at the dimer interface, most notably two hydrogen bonds between the δ-oxygen of D23 and the amide hydrogen of A27 on either subunit, as well as an aromatic ring interaction between Y32 of each subunit.

Table 1. Data processing and refinement statistics for γS disulfide-linked dimer

Data collection	
Wavelength (Å)	0.9763
Space group	*P*1
Cell dimensions	
a, *b*, *c* (Å)	49.63, 52.37, 53.97
α, *β*, *γ* (°)	108.72, 111.46, 105.50
Total reflections	61,796 (5062)
Unique reflections	23,548 (2372)
Multiplicity	2.6 (2.6)
Completeness (%)	93.6 (94.4)
Mean *I*/sigma(*I*)	7.8 (1.3)
Wilson *B*-factor ($Å^2$)	33.3
R-merge	0.032 (0.559)
R-pim	0.022 (0.390)
CC1/2	0.997 (0.757)
Refinement	
R-work/*R*-free	0.2248/0.2716 (0.3067/0.3783)
Number of non-hydrogen atoms	3029
Macromolecules	2892
Water	137
Protein residues	348
RMS (bonds, Å)	0.008
RMS (angles, °)	0.95
Ramachandran preferred (%)	94.45
Ramachandran allowed (%)	4.36
Ramachandran outliers (%)	1.16
Clashscore	6
Average *B*-factor ($Å^2$)	32.55
Macromolecules	32.53
Solvent	32.88
PDB ID	6FD8

Highest-resolution shell is shown in parentheses.

Proteins can adopt quaternary arrangements in solution that are distinct from their crystal structure, for example, the structurally and functionally related βB2-crystallin dimer [35]. Thus, we used SAXS to characterize the structure of the monomer and disulfide-linked γS dimer in solution. The pairwise distance distribution function (*P*(r)) was examined to ensure shape and size differences between γS monomer and dimer were evident in the SAXS data. The *P*(r) of the monomer shows a unimodal distribution consistent with both domains being closely associated with a maximum diameter (D_{max}) of 59 Å and a radius of gyration (R_g) of 18.5 Å. The *P*(r) of the dimer shows a bimodal distribution consistent with

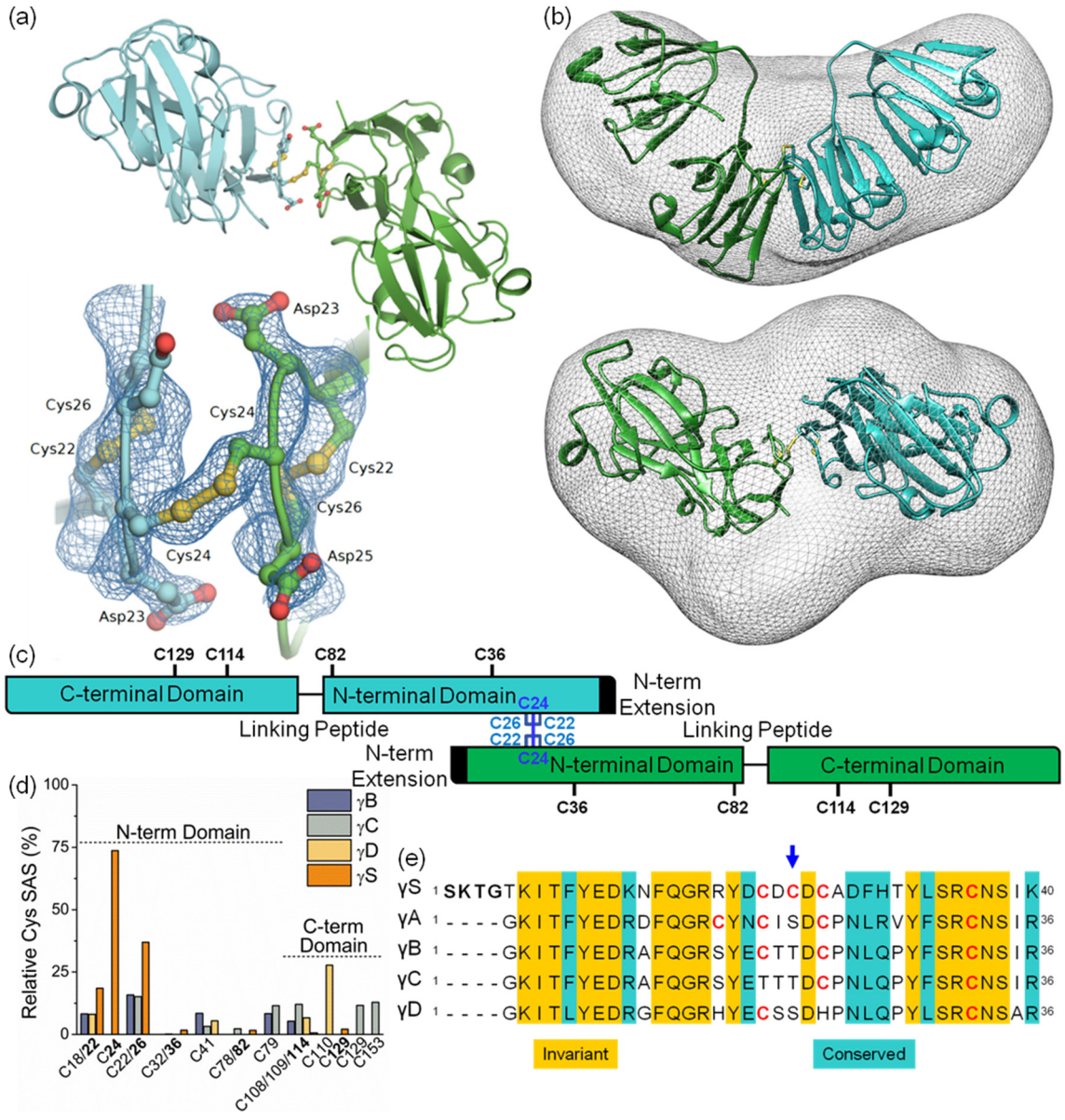

Fig. 1. Structure of the γS dimer. (a) Crystal structure of γS dimer with the inter- (C24) and intramolecular (C22 and C26) disulfide bond arrangement shown as a whole view of the dimer (top) and as a magnified view within the $2mF_o - dF_c$ map (blue lines, contoured at 1.5σ) centered on the intermolecular disulfide bond (bottom). (b) Crystal structure of γS dimer fitted into the *ab initio* SAXS shape envelope (grey line, contoured at 2σ) as shown from a side view (top) and from above (bottom). (c) Linearized schematic of the γS dimer structure with prominent structural features and residues indicated and colored concordantly with the crystal structure above. (d) Comparison of the percentage SAS of all cysteine residues in monomers of γB (PDB: 2JDF), γC (PDB: 2NBR), γD (PDB: 1HK0), and γS (PDB: 2M3T). The structure for γA is not available. SAS is relative to a Gly-Cys-Gly tripeptide in an extended conformation [33]. The positions of cysteine residues in the amino acid sequences of γS and other human γ-crystallins are in bold and normal typeface, respectively. C108 and C109 denote cysteine residues in γC/γD and γB, respectively. (e) Sequence alignment of human γS (residues 1–40) with four other human γ-crystallins highlighting: (i) invariant and chemically conserved amino acid residues as shown in the key; (ii) cysteine residues, C, in bold typeface and red; and (iii) C24 with a blue arrow.

the "V" shape of the disulfide-linked dimer, which exhibits greater distance between the C-terminal domains of each subunit than the alternative non-disulfide linked dimer, giving a D_{max} of 74 Å and a R_g of 24.3 Å (Fig. S1d). A direct comparison of the predicted one-dimensional scattering profiles from the structures of the monomer (PDB: 2M3T) and disulifde-linked dimer with that of the experimentally

obtained scattering data shows that the monomer structure fits well with a χ value of 1.19 (Fig. S1e, light blue). However, the dimer's fit is not as good with a χ value of 2.19 due to a discrepancy in the mid-q range (Fig. S1e, orange). To explore the basis of this structural discrepancy in the dimer, an *ab initio* shape envelope was built using the γS dimer SAXS data within which the crystal structure was fitted (Fig. 1b, top and bottom). The general domain arrangement along the longitudinal axis is consistent with that of the disulfide-linked dimer (Fig. 1b, top), thus verifying the conformation of the biological assembly. There are, however, two protuberances in the transverse plane of the SAXS envelope that correlate with the three-dimensional space that would be sampled by an unstructured and flexible N-terminal extension (Fig. 1b, bottom), encompassing the first four N-terminal residues (Fig. 1c, black, and e, black boldface text) [38]. A similar protuberance is noted in the *ab initio* SAXS envelope of βB2-crystallin dimer due to flexible terminal extensions [35,39]. Given the absence of the first three residues of the N-terminal extension in the crystal structure (due to insufficient electron density) and the high *B*-factor for the fourth residue (G4) (Fig. S1f), it is clear the N-terminal extension maintains flexibility in the dimer. Taken together, these results highlight the source of the discrepancy between the crystal structure and the solution SAXS data as being the N-terminal extension which protrudes from the domain core structure in the dimer (Fig. S1g), as it does in the monomer [40].

C24 is unique to γS and is the most solvent-exposed cysteine in human γ-crystallins

To explore whether this disulfide bonding arrangement observed in human γS is likely to be conserved in γ-crystallins, we compared the sequence of γS to that of human isoforms γA-crystallin (γA), γB-crystallin (γB), γC-crystallin (γC), and γD-crystallin (γD) (Fig. 1e). C22 and C26 (C18 and C22 in other γ-crystallins) are both conserved in γA and γB (Fig. 1e), implying that an intramolecular disulfide bond could form between C18 and C22 in these two γ-crystallins. However, C24 (Fig. 1e, blue arrow) is unique to γS with either serine or threonine substituting for cysteine at the analogous site (position 20) in other isoforms. To assess the relative probability of other human isoforms forming disulfide-linked dimers, we also examined the solvent accessible surface area (SAS) of all cysteines in the monomeric structures of γS, γB, γC, and γD relative to the side-chain SAS of Cys in a Gly-Cys-Gly tripeptide in an extended conformation [33] (Fig. 1d). C24 is significantly more solvent-exposed than any other cysteine in human γ-crystallins, followed by C26, although the latter is unlikely to be involved in the formation of an intermolecular disulfide bond owing to its participation in an intramolecular disulfide bond to C22 (Fig. 1a, bottom, c and d). With the exception of C110 in γD, all other cysteine residues in human γ-crystallins have a SAS of 20% or less (Fig. 1c and d), implying that significant formation of a native disulfide-linked dimer is confined to γS. An interspecies comparison of γS revealed that C24 (Fig. S1c, blue arrow) is highly conserved in eutherians (placental mammals), whereas it is not present in marsupials, birds, reptiles and fish, implying that disulfide-linked dimerization of a variety of eutherian orthologs is possible, as has been observed for bovine γS [31]. Moreover, the absence of C24 in other vertebrates suggests that it is a recent mutation on the evolutionary timescale, arising in a late common ancestor to eutherians (Fig. S1c).

The γS dimer persists in a reducing environment relevant to aging and cataractous lenses

The young human lens is a reducing environment due to the abundance of reduced glutathione (GSH) at a concentration of approximately 6 mM, which diminishes to approximately 2 mM upon aging and to less than 1 mM upon cataract formation [24–26]. We investigated the susceptibility of the γS dimer to dissociation over a range of physiologically relevant reducing environments using analytical SEC. Ratios of GSH and oxidized glutathione (GSSG) to a total concentration of 6 mM were used to modulate the reduction potential of the solution. Analytical SEC profiles showed significant changes over a 72-h period for those samples containing GSH (Fig. S2a). Interestingly, there was a minor linear shift, most prominent at 72 h, in the retention volume of the monomer peak maximum over the GSH:GSSG series (Fig. S2b), which most likely reflects an increase in hydrodynamic size of the monomer due to glutathionylation of the protein (see the following paragraph). From the peak integration values, the percentage of dimer was calculated for each time point and reduction potential, and then plotted against time (Fig. 2a). The results show that over 72 h, the dimer dissociates at an exponential rate that slows with decreasing reducing potential. For example, the dimer was reduced twice as fast by 3 mM GSH, and five times as fast by 6 mM GSH, when compared with 1 mM GSH (Fig. 2b). By 72 h, the percentage of the dimer remained relatively constant over time for all conditions; at 1, 3, and 6 mM GSH, there was 22%, 9%, and 3% dimer remaining, respectively (Fig. 2a). The fully oxidized environment (6 mM GSSG) showed no significant changes in the quantity of disulfide-linked dimer over the experimental time course. Thus, γS is monomeric at GSH:GSSG ratios associated with healthy young lenses, but the dimer becomes increasingly stable as GSH:GSSG

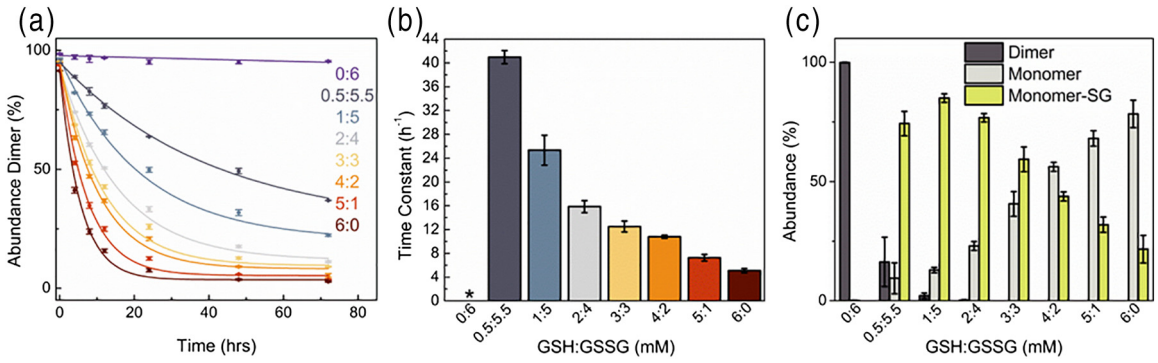

Fig. 2. The effect of glutathione on the abundance, reduction rate and reduction products of the γS dimer. (a) Percentage abundance of the γS dimer with different GSH:GSSG ratios over time as monitored by SEC. The data were fitted to a single exponential decay curve ($R^2 > 0.99$) except for 0:6 GSH:GSSG, which was fitted to a straight line function. (b) Time constant from the single exponential decay curve fitted against the relevant GSH:GSSG ratio. The errors are the standard deviation of two independent repeats. The asterisk denotes data for 0:6 GSH:GSSG that were not fitted to a single exponential decay curve. (c) Relative percentage abundance of the γS dimer, monomer, and glutathionylated monomer (monomer-SG) determined by electrospray ionization MS. The errors are the standard deviation of three independent repeats.

ratios approach those found in aged and cataractous lenses.

MS was used to confirm the analytical SEC results and to detect any chemical modifications to γS upon reduction of the dimer. Masses for the disulfide-linked dimer and the monomer were detected as well as a third species corresponding to *S*-glutathionylated γS monomer (Fig. S2c). Semi-quantitative analysis of all detectable MS species was achieved with a standard curve using purified monomer and dimer (Fig. S2d). It is evident that the dimer ionizes poorly compared to the monomer, thus affecting quantification of the dimer by MS, particularly at lower concentrations, and thereby accounting for discrepancies in its abundance when compared to the concentration sensitive UV-detection in SEC. Nonetheless, the data acquired following 72 h of reduction showed that the abundance of the dimer decreases with increasing reduction potential, alongside a concomitant increase in the abundance of monomeric species (Fig. 2c), concordant with the trend observed by analytical SEC. The abundance of unmodified and *S*-glutathionylated monomer changes across the GSH:GSSG series. At 1:5 GSH:GSSG, for example, 85% of monomer is *S*-glutathionylated; however, this decreases linearly across the series, falling to 22% at 6:0 GSH:GSSG (Fig. 2c). The unmodified monomer consequently shows the inverse trend, consistent with the linear decrease in the monomer's retention volume at higher GSSG concentrations, as noted in SEC (Fig. S2b), implying that glutathionylation occurs via a disulfide exchange mechanism whereby the protein thiol reacts with GSSG. Furthermore, given that no glutathionylation was detected for the dimer (Fig. S2c), glutathionylation occurs at either C22, C24, or C26, which are otherwise disulfide bonded in the dimer. Examination of the unmodified monomer mass peak after reduction of the dimer reveals the highest intensity mass peak shifts with increased reduction potential from 20872 Da to 20874 Da at 1:5 and 6:0 GSH:GSSG, respectively (Fig. S2e). A similar trend can be observed for the *S*-glutathionylated monomer mass peak, largely shifting from 21177 to 21179 Da at 1:5 and 6:0 GSH:GSSG, respectively (Fig. S2f). This 2-Da difference implies that the C22–C26 intramolecular disulfide remains intact after initial reduction of the dimer, but the bond is ultimately reduced at higher reduction potentials. It also implies that γS glutathionylation occurs initially at C24, consistent with it being the most solvent-exposed cysteine (Fig. 1d).

Aggregation propensity is significantly increased when γS forms a disulfide-linked dimer

In view of the link between the oxidation of crystallins and cataract [41] and the increased aggregation propensity of the R14C γD disulfide-linked dimer [32], we investigated the aggregation propensity of the disulfide-linked γS dimer compared to its monomeric counterpart. A light scattering assay at 60 °C showed that the disulfide-linked γS dimer was far more aggregation prone than the monomer from 0.5 to 3.0 mg mL^{-1} (Fig. 3a). On average, the dimer's light scattering maximum was approximately 3.6 times greater than that of the monomer (Fig. 3b). Similarly, the rate of aggregation of the dimer was approximately 2.8 times faster (Fig. 3c). However, the lag time, reflecting the time required for the protein to form a critical nucleus (from which to seed aggregation), was approximately 1.2 times longer for the dimer than for the monomer (Fig. 3d). Thus, while the dimer aggregates faster and to a greater extent,

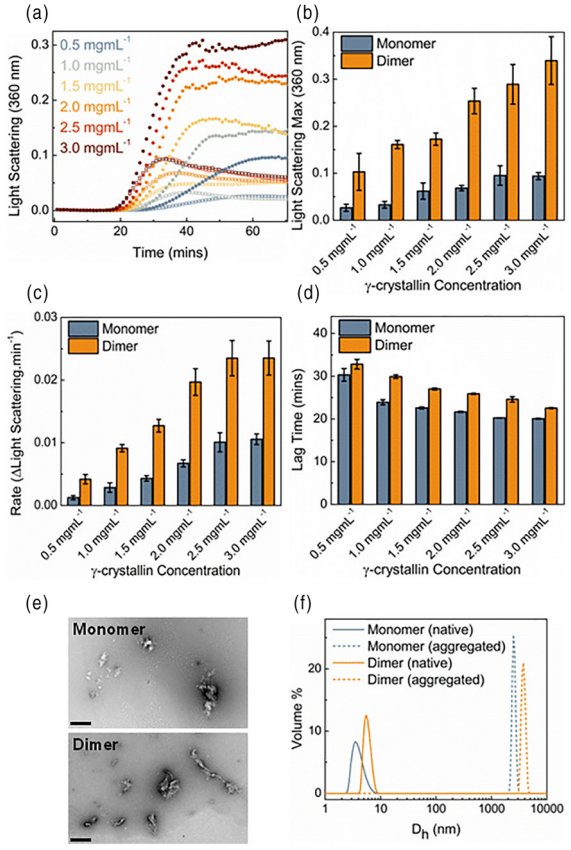

Fig. 3. Aggregation propensity of the γS monomer and dimer. (a) Light scattering (360 nm) assay of γS monomer (hollow squares) and dimer (filled circles) from 0.5 to 3.0 mg mL^{-1} with 0.5 mg mL^{-1} increments. Light scattering kinetic parameters including (b) maximum light scattering, (c) aggregation rate, and (d) lag time of aggregation for γS monomer (light blue) and dimer (orange). Errors are given as the standard deviation of three independent repeats. (e) Negative stain TEM of 1 mg mL^{-1} monomer (top) and dimer (bottom) aggregates formed after 2 h at 60 °C. The scale bar (black, bottom left) represents 500 nm. (f) Dynamic light scattering of 2 mg mL^{-1} native monomer (light blue, solid line) and dimer (orange, solid line) at 25 °C, and aggregated monomer (light blue, dashed line) and dimer (orange, dashed line) after 35 min at 60 °C.

intermolecular interactions in the early stages of aggregation are hindered in comparison to the monomer. The reduced accessibility of specific interfacial residues in the dimer, along with steric considerations, may be factors underlying the extended lag time for the dimer. Transmission electron microscopy (TEM) showed that the aggregates formed by the monomer (Fig. 3e, top) and dimer (Fig. 3e, bottom) appeared essentially amorphous in form with little ordered structure. Dynamic light scattering showed that the aggregates formed by the dimer were, on average, larger than those of the monomer. Initially, the native monomer and dimer measured at 25 °C had an average hydrodynamic diameter (D_h) of 4.0 ± 0.9 and 5.8 ± 0.8 nm, respectively (Fig. 3f, solid line). Upon incubation at 60 °C, there was a rapid, time-dependent increase in D_h for both the monomer and dimer, as anticipated. After 35 min of incubation, the approximate time at which a steady state was observed in the light scattering assay (Fig. 3a), the monomer and dimer exhibited a D_h of 2,541 ± 173 and 3,787 ± 301 nm, respectively (Fig. 3f, dashed line). Thus, the increased light scattering in solution is due, in part, to the increased hydrodynamic size of the dimer aggregates, as well as a potentially higher yield of aggregated protein.

γS dimer undergoes non-cooperative thermal unfolding despite having a similar structure to the monomer

Far-UV circular dichroism (CD) spectra and 8-anilinonaphthalene-1-sulfonic acid (ANS) binding experiments, respectively, showed that the overall secondary structure (Fig. 4a) and surface hydrophobicity (Fig. 4b) of γS are not significantly altered upon dimerization. Indeed, structural alignment of the γS dimer with three other γS structures, that is, the human γS C-terminal domain crystal structure [42] (PDB: 1HA4), the human γS NMR structure [40] (PDB: 2M3T), and the chicken γS crystal structure [43] (PDB: 5VH1) (Fig. 4c–e, respectively), gave C_α RMSD values no greater than 1.9 Å, indicating that the overall fold of the dimer is similar to those previously determined for γS. However, the dimer shows increased intrinsic tryptophan fluorescence relative to that of the monomer (Fig. 4c), suggesting that the fluorescence of one or more of the protein's four tryptophan residues is less efficiently quenched in the dimeric form. Close examination of the environment of the tryptophan residues within the dimer structure revealed that the otherwise highly quenched W162 is not coordinated to a water molecule, in contrast to the truncated γS C-terminal domain structure (PBD: 1HA4), thereby having an impact on the efficient quenching of W162 and potentially accounting for the higher quantum yield [44].

In the absence of evidence of any significant perturbations in the native structure of the disulfide-linked dimer, we examined its thermal stability in an effort to account for its increased aggregation propensity. Four spectroscopic methods, intrinsic tryptophan fluorescence, light scattering, ANS fluorescence, and CD (Fig. 5a–d, respectively), were used to compare the thermal stability of the monomer and dimer. It is apparent in all the unfolding curves that the dimer exhibits biphasic behavior while the monomer is monophasic in its unfolding. It is concluded that the dimer unfolds non-cooperatively, that is, one domain before the other, whereas unfolding of the monomer is concerted (Fig. 5e). Similar thermally induced biphasic unfolding has been noted in the

cataract-associated G18V variant in monomeric γS [45]. From the data in Fig. 5, a mid-point of thermal unfolding (T_m) or aggregation (T_{agg}) was calculated for each transition (Table S1), which showed the mid-point of the dimer's first transition to be lower than that for the single value of the monomer but the second transition to be at a higher temperature. Examination of the difference in T_m values (ΔT_m) between the monomer and those of the dimer and comparison to ΔT_m values reported in the literature for γS and its independent domains (Fig. S3a) implied that the first and second transitions of the dimer represent the unfolding of the N- and C-terminal domains, respectively. For example, while Mills *et al.* [46] reported a ΔT_m for the isolated N- and C-terminal domains of γS of 6.0 °C, the ΔT_m between the first and second transition of the dimer is 6.7 °C (Fig. S3b). Similarly, the ΔT_m between the full-length monomer and each domain [46] is comparable to the ΔT_m between the monomer and each transition of the dimer, implying that domain stability differences are largely conserved and, moreover, that unfolding of the N-terminal domain precedes that of the C-terminal domain in the γS dimer (Fig. 5f). Interestingly, the G18V variant, which also exhibits biphasic thermal unfolding, gave a ΔT_m between its first and second transition of 8.0 °C [45], comparable with the ΔT_m of 7.9 °C between the first and second transition of the dimer (Fig. S3c). Potentially, therefore, the biphasic unfolding induced in γS by the cataract-associated G18V mutation parallels the behavior induced by disulfide-linked dimerization.

Discussion

The evidence for cysteine oxidation, including disulfide crosslinks, between crystallin proteins in aging and cataractous lenses is extensive [16,17, 21–23,47]. Previous studies have shown that disulfide bonds can form *in vitro* in γ-crystallins [18,31, 32,48], but most studies do not demonstrate the ability for these disulfides to be viable in a reducing environment commensurate with that of the lens. Human lens GSH concentrations decrease with age

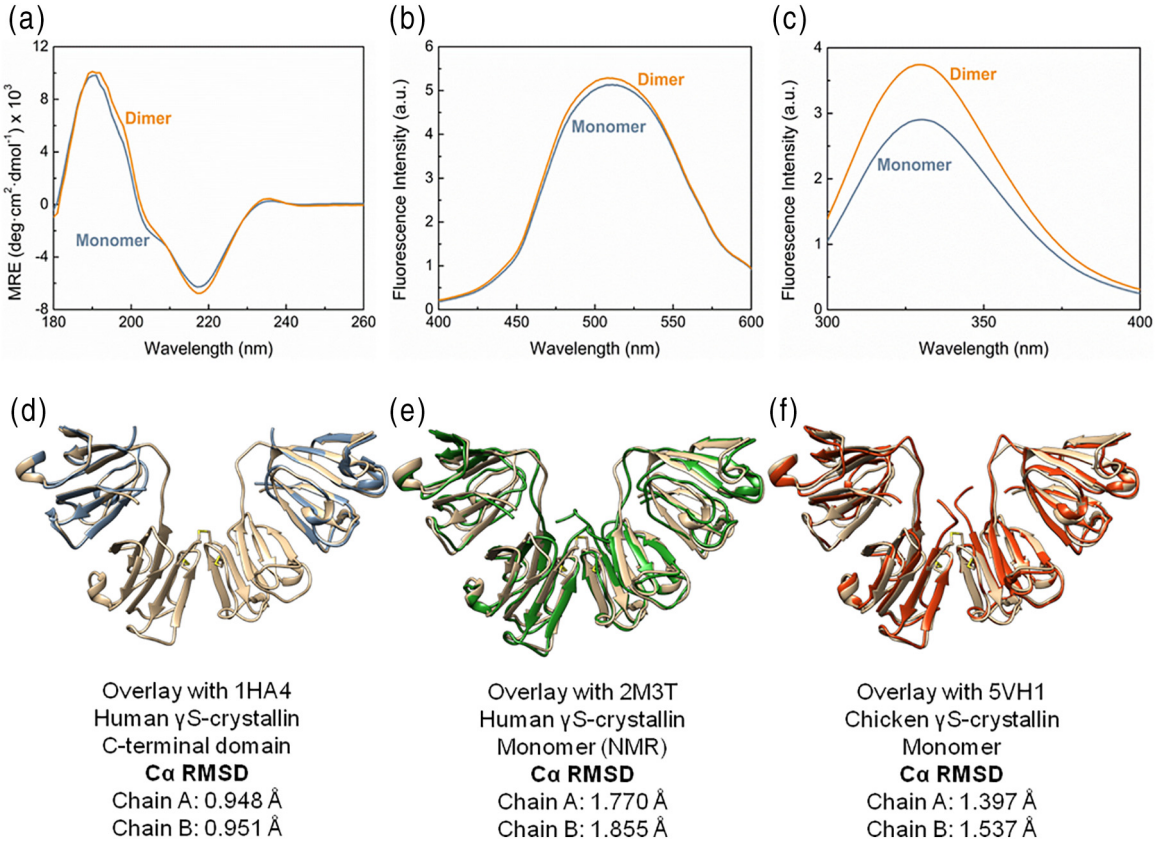

Fig. 4. Comparison of the secondary structure, surface hydrophobicity and overall conformation of the γS monomer, γS dimer and related structures. (a) Far-UV CD, (b) ANS fluorescence, and (c) tryptophan fluorescence spectra of γS monomer (light blue) and dimer (orange). Structural overlay between human γS dimer (beige) and (d) human γS C-terminal domain crystal structure (blue; PDB: 1HA4), (e) human γS NMR structure (green; PDB: 2M3T) and (f) chicken γS crystal structure (red; PDB: 5VH1). The RMSD is given as a quantitative measure of structural similarity.

from approximately 6 to 2 mM and can fall below 1 mM in cataract [24–26]. We have shown that the γS disulfide-linked dimer becomes increasingly stable at GSH concentrations found in aging and cataractous lenses. While these studies were completed at physiological GSH concentrations, it is worth noting that the concentration of γS in the lens is likely to be in the order of 100 times more than that studied here [6,49]. Furthermore, the aging, GSH-depleted lens would need to contend with the stress associated with the oxidation of other lenticular components [50]. Thus, we consider the experimental values of dimer abundance determined herein to be conservative estimates in relation to the prevalence of the disulfide-linked γS dimer *in vivo*.

Glutathionylation of crystallin proteins in normal and cataractous human lenses has been noted numerous times with the prevalence of this modification being positively correlated with aging [24,51–53]. γS extracted from the human lens is *S*-glutathionylated at two sites, with one modification at either C22, C24, or C26 and another at C82 [30]. We observed a single glutathionylation of γS by MS and inferred that the modification occurred at C24, consistent with its high solvent exposure (Fig. 1d). In natively folded γS, C82 is unlikely to be glutathionylated due to its very low solvent exposure, and as such, glutathionylation at C82 *in vivo* is likely an indicator of partial unfolding of the N-terminal domain. The abundance of glutathionylated γS monomer is directly proportional to the concentration of GSSG (Fig. 2c and S2b), indicative of mixed disulfide formation via an exchange mechanism which has been previously noted as the preferred mechanism for the addition of glutathione to crystallins [52,54]. Furthermore, the amount of glutathionylation at 6:0 GSH:GSSG is likely due to the reduction of dimer consequently forming GSSG. This mechanism is consistent with C24 being present largely in the reduced thiol (protonated) form at physiological p*H*, due to an elevated pK_a value as a result of flanking negatively charged aspartyl residues in the "DCDCDC" motif from residues 21–26 [31]. A disulfide exchange mechanism also has implications for the formation of the γS dimer, which could foreseeably arise via a reaction between *S*-glutathionylated and unmodified γS monomers, resulting in the formation of a protein-protein disulfide link and GSH (Fig. 6). Indeed, γS has been proposed to function as a "redox sink" in the aging lens, that is, acting as a reducing agent to consume GSSG and replenish GSH levels in the process of forming disulfide-linked dimers [6,31]. However, given the enhanced aggregation propensity of the γS dimer, such replacement would be a trade-off in order to maintain a reducing environment in the lens.

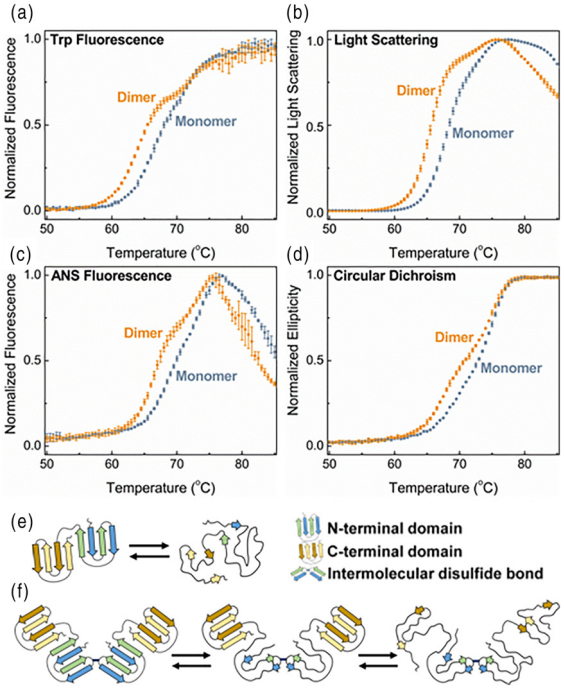

Fig. 5. Thermal stability of the γS monomer and dimer. The γS monomer (light blue) and dimer (orange) were monitored using (a) tryptophan fluorescence (Trp) (ratio 345/329 nm), (b) light scattering at 360 nm, (c) ANS fluorescence at 480 nm, and (d) CD at 218 nm. Curves are the average of three independent repeats, and the errors are given as standard deviation. (e) Schematic diagram depicting how the γS monomer unfolds cooperatively, while the γS dimer (f) unfolds non-cooperatively, initially via its N-terminal domain. Structural features of the monomer and dimer are denoted in the key adjacent to panel e.

The link between PTMs, particularly oxidation, disulfide bond formation, and cataract is prevalent, with a prevailing sentiment being that the formation of age-related cataract is a function of PTMs, heat, and time [14–16]. Single-residue mutations such as G18V in γS [45] and R14C (which can form disulfide-linked dimers) in γD [32] have a heightened aggregation propensity and are associated with cataract. However, both variants are structurally comparable to their wild-type counterparts. Similarly, the γS disulfide-linked dimer is also far more aggregation prone, but its structure is not altered when compared to the monomer. The thermal denaturation of the γS dimer also resembles that of the cataract-associated G18V variant [45]. Overall, thermal denaturation indicates that disulfide-linked dimerization of γS decouples the unfolding cooperativity of the N- and C-terminal domains. However, while a loss of cooperativity is evident, the relative stability difference between the N- and C-terminal domains does not appear to be affected upon comparison with the isolated N- and C-terminal domains (Fig. S3a). Possible causes of this are likely to be related to subtle changes in domain flexibility and altered interactions with water upon dimerization. Indeed, molecular dynamics studies on

homology structures of wild-type and G18V γS reveal that changes in inter-strand salt-bridge interactions accompany changes in dynamics that allow water permeable openings in the N-terminal domain of G18V [55]. This could further disrupt bonding networks that lead to a loss of the cooperative unfolding mechanism between the two domains as has been noted for this cataract-associated variant [45]. Furthermore, NMR studies on murine cataract-associated F9S, which also exhibits non-cooperative domain unfolding, show changes to the tryptophan (a "Trp corner") involved in hydrogen bonding and stabilization of a β-turn in the N-terminal domain. As Trp or Tyr corners have been intimately linked to the folding/unfolding mechanism of Greek-key folds [56,57], this could highlight an additional role in the maintenance of folding/unfolding cooperativity.

The biphasic unfolding of the dimer indicates a thermodynamically stabilized intermediate, which is likely characterized by an unfolded N-terminal domain and a folded C-terminal domain, as has been observed in other destabilized γ-crystallins [18,45,58–60]. Consistent with this, molecular dynamics simulations have implied that γD can aggregate through domain swapping via a partially folded intermediate characterized by an unfolded N-terminal domain but an otherwise folded C-terminal domain [61]. Indeed, the γS disulfide-linked dimer is far more aggregation prone compared to the monomer, displaying ostensibly amorphous looking aggregates via TEM (Fig. 3e, bottom). However, it has been demonstrated that partially ordered P23T γD aggregates are indistinguishable from amorphous aggregates when viewed by TEM [62], indicating that further investigation into the substructure of the aggregates observed here is needed to obtain a more complete understanding of their molecular underpinnings. The present study suggests that the disulfide-linked γS dimer is highly analogous to the G18V and dimer-forming R14C variants, which are both associated with progressive juvenile-onset cataract [32,45]. Such cataract-associated variants therefore appear to exhibit structural markers similar to those that may emerge in wild-type γ-crystallins later in life due to aging, for example, the formation of non-native disulfides [18]. We propose that oxidation and subsequent dimerization of γS preferentially destabilizes its N-terminal domain, as is evident in G18V, resulting in a thermodynamically stable intermediate that exhibits increased aggregation and thereby exacerbates light scattering associated with age-related cataract (Fig. 6).

In summary, we have characterized an oxidative PTM of human γS and provided a molecular basis for its role in age-related cataract. Determination of the crystal structure of the oxidation product showed γS in the form of a dimer linked via an intermolecular disulfide bond at C24 [31] and also revealed an intramolecular disulfide between C22 and C26. No gross conformational changes were observed upon oxidation. We have demonstrated that this PTM is stable at GSH concentrations akin to those in aged and cataractous lenses and the PTM increases the propensity of γS to aggregate. Along with other conformational features shared by the γS dimer and cataract-associated variants, these findings strongly suggest that the occurrence of this PTM in the aging lens leads to or worsens the severity of cataract. The mechanism outlined here may apply more broadly to other crystallin proteins that undergo oxidative PTMs as part of the oxidation-driven aggregation cascade that underlies age-related cataract.

Materials and Methods

Production of γS monomer and dimer

A pET43.1 plasmid encoding recombinant human γS (178 amino acids; UniProt P22914) was purchased from Genscript and expressed in BL21(DE3) *E. coli* cells. Cells were cultured initially at 37 °C for 4–5 h. Expression was then induced with 500 μM IPTG, and the cell culture was incubated overnight at 30 °C. Cells were pelleted, resuspended in DEAE column buffer (20 mM Tris–HCl, pH 8.0), and lysed using sonication. The cell lysate was loaded onto an anion-exchange column (HiPrep DEAE FF 16/10; GE Healthcare) and a peak containing γS eluted in the flow-through. Fractions containing predominantly γS were concentrated to ~1 mL, loaded onto a preparative SEC column (HiLoad 16/600 Superdex 75 pg; GE Healthcare) and separated in PBS (50 mM sodium phosphate, 100 mM NaCl, pH 7.0. The peak corresponding to monomeric γS was collected. This initial fraction of monomeric γS was concentrated to a minimum of 20 mg mL^{-1} using an Amicon Ultra-15 Centrifugal Filter Unit (Merck Millipore) and left at 4 °C for 1 week to allow for large-scale dimerization of γS (up to 60% of the total protein). Monomeric and dimeric forms of γS were then purified by two sequential separations via preparative SEC, eluting with 20 mM sodium phosphate buffer (pH 7.0). Within 30 min of elution, respective fractions of monomer and dimer were frozen with dry ice in 0.2–0.5 mL aliquots at protein concentrations of 4-8 mg mL^{-1}. Aliquots were thawed immediately prior to use.

Crystallization, data collection, and refinement

Purified γS dimer was buffer exchanged to 10 mM HEPES (pH 7.2) and concentrated to 10 mg mL^{-1}. Crystals were obtained by vapor diffusion in sitting drops containing 0.2 M sodium tartrate dibasic dihydrate (pH 7.3) and 20% w/v polyethylene glycol

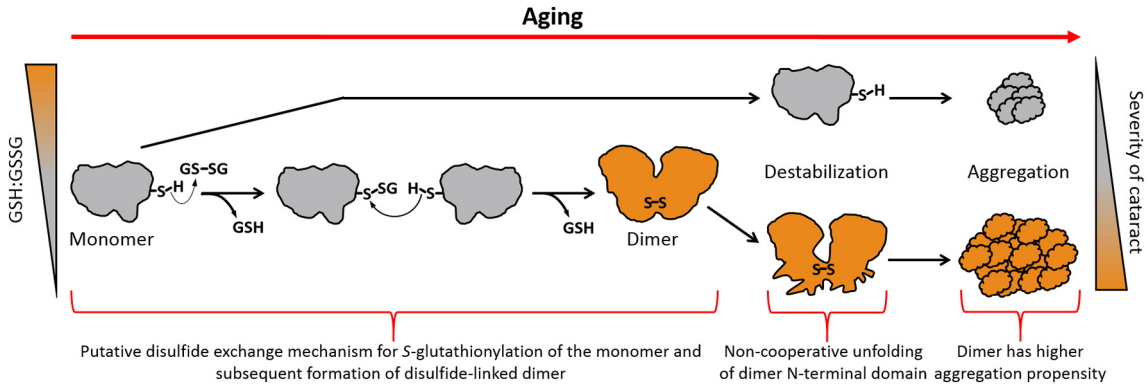

Fig. 6. Putative schematic representation of the process of oxidation/dimerization, destabilization, and aggregation of human γS.

3350 (Hampton Research). For cryoprotection, drops were supplemented with 30% w/v polyethylene glycol 3350 and crystals were subsequently vitrified by submersion in liquid nitrogen. Diffraction data were collected at a wavelength of 0.9763 Å on the MX2 beam line of the Australian Synchrotron. Diffraction data were indexed, scaled, and integrated using XDS [63]. Phases were obtained, via molecular replacement, using PhaserMR [64] with the crystal structure of chicken γS [43] (PDB 5VH1) as the search model. Cycles of refinement and manual rebuilding were completed using PHENIX and Coot, respectively [65,66].

SAXS measurements and *ab initio* envelope reconstruction

Experiments were conducted on a NanoSTAR II SAXS (Bruker) with a rotating anode Cu Kα radiation source at a wavelength of 1.541 Å and using a q range of 0.013–0.39 $Å^{-1}$. Samples of γS monomer (3 mg mL^{-1}) and dimer (6 mg mL^{-1}) were prepared in 20 mM sodium phosphate (pH 7.0). Samples were loaded into a sealed 2 mm quartz capillary cell and placed under vacuum. Scattering was collected in 1-h increments for a total of 4 h in a temperature controlled sample environment at 25 °C. No change in the scattering of the monomer or dimer was observed over the 4-h acquisition period. The data were averaged and subtracted from the scattering of the buffer using PRIMUS [67]. Low q points near the beam stop were excluded. The P(r) and the R_g were calculated using GNOM [68]. Using CRYSOL, the scattering profiles of the γS monomer (PBD: 2M3T) and dimer structures (PDB: 6FD8) were modeled and fitted to their respective experimental scattering profiles [69]. Using GASBOR [70], 15 *ab initio* shape envelopes were initially generated which were then aligned, filtered, and averaged using the DAMAVER suite [71]. This averaged structure underwent refinement using DAMMIN [72] to produce the final *ab initio* envelope. Using UCSF Chimera [73], the final envelope was converted to a volumetric map, contoured to 2σ and aligned with the γS dimer crystal structure, giving a correlation coefficient for the fit of 0.89.

Structural and sequence analysis

The SAS of all cysteine residues in the monomeric structures of γB (PDB: 2JDF), γC (PDB: 2NBR), γD (PDB: 1HK0), and γS (PDB: 2M3T) was investigated using UCSF Chimera [73]. In the case of NMR-derived structures (γC and γS), the SAS was averaged across all conformers. The SAS was converted to a percentage relative to the side-chain SAS of a Cys in a Gly-Cys-Gly tripeptide in an extended conformation [33]. Sequence alignments were generated using the Clustal Omega server [74] and colored according to the consensus symbols generated on the basis of their Gonnet PAM 250 matrix score [≤0.5 (.) weakly conserved (green); >0.5 (:) strongly conserved (blue); = 1.0 (*) invariant (orange)]. The phylogenetic tree was constructed using the National Center for Biotechnology Information taxonomy database. Structural overlay of the γS dimer was completed using UCSF Chimera and the RMSD of the C_α atoms was reported as the measure of structural similarity between other γS structures with the PDB accession codes 1HA4, 2M3T, and 5VH1.

Reduced and oxidized glutathione treatments of γS dimer

The γS dimer at a concentration of 0.3 mg mL^{-1} was incubated in filtered (0.44 μm) 20 mM sodium phosphate (pH 7.0) at room temperature with different ratios of GSH (G4251, Sigma) and GSSG (G4376, Sigma). GSH:GSSG molar ratios were 0:6, 0.5:5.5, 1:5, 2:4, 3:3, 4:2, 5:1, and 6:0, maintaining a 6 mM final concentration of glutathione.

Analytical SEC

γS dimer was prepared with GSH:GSSG ratios as previously detailed. Following treatment for 0, 4, 8, 12, 24, 48, and 72 h, γS dimer was separated into its monomeric and dimeric components using a Superdex 75 10/300 GL SEC (GE Healthcare) column attached to an ÄKTA Pure FPLC (GE Healthcare) with UV absorbance (280 nm) detection. Monomer and dimer peaks were baseline corrected and integrated using Unicorn 6.3 software (GE Healthcare). All experiments were performed at room temperature using filtered (0.44 μm) 20 mM sodium phosphate (pH 7.0) at a flow rate of 0.8 mL min^{-1}.

Mass spectrometry

Experiments were performed using an Orbitrap Elite mass spectrometer equipped with a HESI-II electrospray ionization source coupled to an UltiMate 3000 UHPLC (Thermo Scientific). γS dimer was prepared with GSH:GSSG ratios as previously detailed. Samples (7 μL) were injected into the mass analyzer following treatment for 24 and 72 h. A mass range of 200 to 4000 at a resolution of 240,000 was acquired. The data were extracted and analyzed using Thermo Xcalibur Qual software. Peaks corresponding to the monomer, monomer–glutathione adduct, and dimer were plotted as intensity *versus* mass (Fig. S2c) and quantified (Fig. 2c) using standard curves. Standard curves were generated using purified γS monomer and dimer at approximately 0.02, 0.05, 0.1, 0.2, 0.3, 0.35, and 0.4 mg mL^{-1} and mixed to achieve a total concentration of approximately 0.4 mg mL^{-1} (Fig. S2d). The standard curve samples were mixed to diminish any effects on the final intensity count due to ionization transfer between monomer and dimer species during experiments where the monomer was being generated from the dimer. The ionization intensity of the monomer–glutathione adduct was assumed to be the same as that of the monomer.

Transmission electron microscopy

Samples for TEM were prepared by adding 2 μL of 1 mg mL^{-1} γS monomer or dimer incubated for 2 h at 60 °C to Formvar and carbon-coated copper grids (ProSciTech, Australia). The grids were then washed three times with 10 μL of Milli-Q water and negatively stained with 10 μL of uranyl acetate (2% w/v). Samples were viewed using a Hitachi H7100FA transmission electron microscope (Tokyo, Japan).

Thermal stability

Experiments were performed using an Applied Photophysics Chirascan spectrophotometer attached to a Quantum Northwest TC 125 PELTIER temperature controller. CD measurements were acquired in a 0.1 cm pathlength quartz cuvette, while light scattering and Trp/ANS fluorescence experiments were acquired in a 1 cm pathlength quartz cuvette. All cuvettes were fitted with stoppers to prevent evaporation. Proteins were prepared in 20 mM sodium phosphate (pH 7.0) at a protein concentration of 0.3 mg mL^{-1}. Thermal stability was assessed by ramping the temperature in 0.5 °C increments from 25 to 90 °C. At each increment, measurements at a single wavelength were acquired for 1.5 s for 5 repeats with a 30 s equilibration between each temperature increment. Trp and ANS fluorescence were measured at excitation wavelengths of 295 and 350 nm, respectively. The concentration of ANS used was 300 μM. The acquisition wavelengths were 218 nm (CD), 345/329 nm (Trp fluorescence), 360 nm (light scattering), and 480 nm (ANS fluorescence). Experiments were performed in triplicate. A single or double Boltzmann sigmoidal function was fitted to the thermal unfolding curves to obtain the T_m or T_{agg} values.

Aggregation assay

Kinetic aggregation assays were performed using a Biotek Synergy 2 microplate reader. Protein aggregation was induced at 60 °C and monitored using light scattering at 360 nm. A "slow shaking" setting was engaged for the duration of the assay. The aggregation of γS monomer and dimer was studied at 0.5, 1.0, 1.5, 2.0, 2.5, and 3.0 mg mL^{-1}. Aggregation kinetics were fitted to a single Boltzmann function using Origin (OriginLab Corporation) and the fitting parameters were used to calculate the lag time and rate of aggregation as previously described [75].

Dynamic light scattering

Experiments were performed using a Zetasizer Nano ZS (Malvern Instruments) with a built-in PELTIER temperature control system. A standard He–Ne laser operating at a wavelength of 633 nm and a scattering detection angle of 173° (backscattering) was used for data collection. γS monomer and dimer solutions were filtered through Millex Durapore (0.22 μm) filters and subsequently loaded into a semi-micro quartz cuvette fitted with a stopper. The final concentration of protein was 2 mg mL^{-1} in 20 mM sodium phosphate (pH 7.0). Size measurements of the native monomer and dimer were performed at 25 °C. The sample was then placed at 60 °C, and aggregation was monitored continuously until the protein was fully aggregated. Size measurements collected within each 2-min increment were averaged. Figure 3e shows data for the fully aggregated sample acquired after 35 min, consistent with the time at which a steady state is reached in aggregation assays monitored by light scattering.

SEC with multi-angle light scattering detection

γS monomer and dimer were loaded onto a Superdex 75 10/300 GL SEC (GE Healthcare) column in filtered (0.22 μm) 20 mM sodium phosphate (pH 7.0) with multi-angle light scattering (DAWN HELEOS 8; Wyatt Technologies) and refractive index detection (Optilab rEX; Wyatt Technologies). The multi-angle detectors were normalized using monomeric bovine serum albumin (Sigma, A1900). A *dn*/*dc* value of 0.1983 mL g^{-1} for human γS [3] was used. The data were processed using ASTRA (Wyatt Technologies).

Spectroscopy

CD and ANS fluorescence spectra were acquired in 2 mM sodium phosphate (pH 7.0), while Trp fluorescence was acquired in 20 mM sodium phosphate (pH 7.0). All experiments were performed at a concentration of 0.3 mg mL^{-1} at 25 °C. CD spectra were acquired from 180 to 260 nm, ANS fluorescence from 400 to 600 nm, and Trp fluorescence from 300 to 400 nm. Fluorescence parameters were the same as those used for the thermal stability experiments, except that the excitation bandwidth was set to 5 nm for ANS fluorescence experiments. Three repeats were acquired with a step width of 1 nm for 4 s. These parameters were used for three independent experiments, which were averaged to produce the final spectrum.

Data deposition and accession numbers

The coordinates and structure factors have been deposited in the Protein Data Bank with accession number PDB ID 6FD8. SAXS data were deposited in the Small Angle Scattering Biological Data Bank (SASBDB) under the accession codes SASDEZ6 (gamma-crystallin S disulfide-linked dimer) and SASDE27 (gamma-crystallin S monomer).

Supplementary data to this article can be found online at https://doi.org/10.1016/j.jmb.2018.12.005.

CRediT authorship contribution statement

David C. Thorn: Conceptualization, Formal analysis, Investigation, Writing - review & editing. **Aidan B. Grosas:** Conceptualization, Data curation, Formal analysis, Investigation, Visualization, Writing - original draft, Writing - review & editing. **Peter D. Mabbitt:** Formal analysis, Writing - review & editing, . **Nicholas J. Ray:** Investigation. **Colin J. Jackson:** Formal analysis, Resources, Supervision, Writing - review & editing. **John A. Carver:** Conceptualization, Funding acquisition, Project administration, Supervision, Writing - review & editing.

Acknowledgments

We thank Prof. Roger Truscott and Ms. Jen Xiang for insightful discussions. We acknowledge Dr. Paul Carr for helpful discussions related to protein crystallography. The Centre for Advanced Microscopy at ANU is acknowledged for their assistance with TEM. We are grateful to Dr. Adam Carroll and the team at the Joint Mass Spectrometry Facility, ANU, for help and guidance in performing and designing mass spectrometry experiments. We are grateful to Dr. Robert Knott at the Australian Nuclear Science and Technology Organisation, Lucas Heights, for his assistance with SAXS measurements. A.B.G. is supported by an Australian Postgraduate Award. D.C.T. is supported by a grant from the National Health and Medical Research Council of Australia (Grant No. 1068087) awarded to J.A.C.

Conflict of Interest: The authors declare no conflict of interest.

Received 31 October 2018;
Accepted 5 December 2018
Available online 13 December 2018

Keywords:
crystallin;
disulfide bond;
dimer;
oxidation;
cataract

†D.C.T. and A.B.G. contributed equally to this work.

Current address: P.D. Mabbitt, MRC Protein Phosphorylation and Ubiquitination Unit, University of Dundee, Dundee, UK.

Abbreviations used:
γS, γS-crystallin; PTM, post-translational modification; MS, mass spectrometry; SAS, solvent accessible surface area; GSH, reduced glutathione; GSSG, oxidized glutathione; ANS, 8-anilino-1-naphthalenesulfonic acid; CD, circular dichroism; TEM, transmission electron microscopy.

References

[1] M. Delaye, A. Tardieu, Short-range order of crystallin proteins accounts for eye lens transparency, Nature 302 (1983) 415.

[2] A. Ponce, C. Sorensen, L. Takemoto, Role of short-range protein interactions in lens opacifications, Mol. Vis. 12 (2006) 879–884.

[3] H. Zhao, P.H. Brown, M.T. Magone, P. Schuck, The molecular refractive function of lens γ-crystallins, J. Mol. Biol. 411 (2011) 680–699.
[4] H.P. Driessen, P. Herbrink, H. Bloemendal, W.W. de Jong, Primary structure of the bovine β-crystallin Bp chain: internal duplication and homology with γ-crystallin, Eur. J. Biochem. 121 (1981) 83–91.
[5] D. Hogg, L. Tsui, M. Gorin, M. Breitman, Characterization of the human β-crystallin gene Hu β A3/A1 reveals ancestral relationships among the beta gamma-crystallin superfamily, J. Biol. Chem. 261 (1986) 12420–12427.
[6] H. Bloemendal, W. de Jong, R. Jaenicke, N.H. Lubsen, C. Slingsby, A. Tardieu, Ageing and vision: structure, stability and function of lens crystallins, Prog. Biophys. Mol. Biol. 86 (2004) 407–485.
[7] T. Blundell, P. Lindley, L. Miller, D. Moss, C. Slingsby, I. Tickle, B. Turnell, G. Wistow, The molecular structure and stability of the eye lens: X-ray analysis of γ-crystallin II, Nature 289 (1981) 771.
[8] G. Inana, J. Piatigorsky, B. Norman, C. Slingsby, T. Blundell, Gene and protein structure of a β-crystallin polypeptide in murine lens: relationship of exons and structural motifs, Nature 302 (1983) 310.
[9] C. Slingsby, N.J. Clout, Structure of the crystallins, Eye 13 (1999) 395.
[10] S. Bassnett, Lens organelle degradation, Exp. Eye Res. 74 (2002) 1–6.
[11] N. Lynnerup, H. Kjeldsen, S. Heegaard, C. Jacobsen, J. Heinemeier, Radiocarbon dating of the human eye lens crystallines reveal proteins without carbon turnover throughout life, PLoS One 3 (2008), e1529.
[12] B.H. Toyama, J.N. Savas, S.K. Park, M.S. Harris, N.T. Ingolia, J.R. Yates III, M.W. Hetzer, Identification of long-lived proteins reveals exceptional stability of essential cellular structures, Cell 154 (2013) 971–982.
[13] M.G. Friedrich, R.J. Truscott, Membrane association of proteins in the aging human lens: profound changes take place in the fifth decade of life, Invest. Ophthalmol. Vis. Sci. 50 (2009) 4786–4793.
[14] K.L. Moreau, J.A. King, Protein misfolding and aggregation in cataract disease and prospects for prevention, Trends Mol. Med. 18 (2012) 273–282.
[15] R.J. Truscott, M.G. Friedrich, The etiology of human age-related cataract. Proteins don't last forever, Biochim. Biophys. Acta Gen. Subj. 1860 (2016) 192–198.
[16] R.J. Truscott, Age-related nuclear cataract—oxidation is the key, Exp. Eye Res. 80 (2005) 709–725.
[17] P.G. Hains, R.J. Truscott, Proteomic analysis of the oxidation of cysteine residues in human age-related nuclear cataract lenses, Biochim. Biophys. Acta Proteins Proteom. 1784 (2008) 1959–1964.
[18] E. Serebryany, J.C. Woodard, B.V. Adkar, M. Shabab, J.A. King, E.I. Shakhnovich, An internal disulfide locks a misfolded aggregation-prone intermediate in cataract-linked mutants of human γD-crystallin, J. Biol. Chem. 291 (2016) 19172–19183.
[19] E. Serebryany, T. Takata, E. Erickson, N. Schafheimer, Y. Wang, J.A. King, Aggregation of Trp > Glu point mutants of human gamma-D crystallin provides a model for hereditary or UV-induced cataract, Protein Sci. 25 (2016) 1115–1128.
[20] S. Ramkumar, X. Fan, B. Wang, S. Yang, V.M. Monnier, Reactive cysteine residues in the oxidative dimerization and Cu^{2+} induced aggregation of human γD-crystallin: implications for age-related cataract, Biochim. Biophys. Acta Mol. Basis Dis. 1864 (2018) 3595–3604.
[21] R.J. Truscott, R.C. Augusteyn, Oxidative changes in human lens proteins during senile nuclear cataract formation, Biochim. Biophys. Acta 492 (1977) 43–52.
[22] A. Spector, D. Roy, Disulfide-linked high molecular weight protein associated with human cataract, Proc. Natl. Acad. Sci. U. S. A. 75 (1978) 3244–3248.
[23] S.R.A. Hanson, A. Hasan, D.L. Smith, J.B. Smith, The major in vivo modifications of the human water-insoluble lens crystallins are disulfide bonds, deamidation, methionine oxidation and backbone cleavage, Exp. Eye Res. 71 (2000) 195–207.
[24] J.J. Harding, Free and protein-bound glutathione in normal and cataractous human lenses, Biochem. J. 117 (1970) 957–960.
[25] A. Kamei, Glutathione levels of the human crystalline lens in aging and its antioxidant effect against the oxidation of lens proteins, Biol. Pharm. Bull. 16 (1993) 870–875.
[26] L.M. Bova, M.H.J. Sweeney, J.F. Jamie, R.J.W. Truscott, Major changes in human ocular UV protection with age, Invest. Ophthalmol. Vis. Sci. 42 (2001) 200–205.
[27] K.J. Lampi, Z. Ma, M. Shih, T.R. Shearer, J.B. Smith, D.L. Smith, L.L. David, Sequence analysis of βA3, βB3, and βA4 crystallins completes the identification of the major proteins in young human lens, J. Biol. Chem. 272 (1997) 2268–2275.
[28] J.A. Thomson, R.C. Augusteyn, Ontogeny of human lens crystallins, Exp. Eye Res. 40 (1985) 393–410.
[29] V.N. Lapko, D.L. Smith, J.B. Smith, *S*-methylated cysteines in human lens γS-crystallins, Biochemistry 41 (2002) 14645–14651.
[30] J. Craghill, A.D. Cronshaw, J.J. Harding, The identification of a reaction site of glutathione mixed-disulphide formation on γS-crystallin in human lens, Biochem. J. 379 (2004) 595–600.
[31] F. Skouri-Panet, F. Bonneté, K. Prat, O.A. Bateman, N.H. Lubsen, A. Tardieu, Lens crystallins and oxidation: the special case of γS, Biophys. J. 89 (2001) 65–76.
[32] A. Pande, J. Pande, N. Asherie, A. Lomakin, O. Ogun, J. A. King, N.H. Lubsen, D. Walton, G.B. Benedek, Molecular basis of a progressive juvenile-onset hereditary cataract, Proc. Natl. Acad. Sci. U. S. A. 97 (2000) 1993–1998.
[33] S. Miller, J. Janin, A.M. Lesk, C. Chothia, Interior and surface of monomeric proteins, J. Mol. Biol. 196 (1987) 641–656.
[34] M.A. Smith, O.A. Bateman, R. Jaenicke, C. Slingsby, Mutation of interfaces in domain-swapped human βB2-crystallin, Protein Sci. 16 (2007) 615–625.
[35] Z. Xi, M.J. Whitley, A.M. Gronenborn, Human βB2-crystallin forms a face-en-face dimer in solution: an integrated NMR and SAXS study, Structure 25 (2017) 496–505.
[36] B. Bax, R. Lapatto, V. Nalini, H. Driessen, P. Lindley, D. Mahadevan, T. Blundell, C. Slingsby, X-ray analysis of βB2-crystallin and evolution of oligomeric lens proteins, Nature 347 (1990) 776.
[37] E. Krissinel, K. Henrick, Inference of macromolecular assemblies from crystalline state, J. Mol. Biol. 372 (2007) 774–797.
[38] P.G. Cooper, J.A. Carver, J.A. Aquilina, G.B. Ralston, R.J. Truscott, A ^{1}H NMR spectroscopic comparison of γS- and γB-crystallins, Exp. Eye Res. 59 (1994) 211–220.

[39] J.A. Carver, P.G. Cooper, R.J.W. Truscott, 1H-NMR spectroscopy of βB2-crystallin from bovine eye lens, Eur. J. Biochem. 213 (1993) 313–320.
[40] C.N. Kingsley, W.D. Brubaker, S. Markovic, A. Diehl, A.J. Brindley, H. Oschkinat, R.W. Martin, Preferential and specific binding of human αB-crystallin to a cataract-related variant of γS-crystallin, Structure 21 (2013) 2221–2227.
[41] A. Taylor, K.J.A. Davies, Protein oxidation and loss of protease activity may lead to cataract formation in the aged lens, Free Radic. Biol. Med. 3 (1987) 371–377.
[42] A.G. Purkiss, O.A. Bateman, J.M. Goodfellow, N.H. Lubsen, C. Slingsby, The X-ray crystal structure of human γS-crystallin C-terminal domain, J. Biol. Chem. 277 (2002) 4199–4205.
[43] V. Sagar, S.K. Chaturvedi, P. Schuck, G. Wistow, Crystal structure of chicken γS-crystallin reveals lattice contacts with implications for function in the lens and the evolution of the βγ-crystallins, Structure 25 (2017) 1068-78.e2.
[44] J. Chen, P.R. Callis, J. King, Mechanism of the very efficient quenching of tryptophan fluorescence in human γD- and γS-crystallins: the γ-crystallin fold may have evolved to protect tryptophan residues from ultraviolet photodamage, Biochemistry 48 (2009) 3708–3716.
[45] Z. Ma, G. Piszczek, P.T. Wingfield, Y.V. Sergeev, J.F. Hejtmancik, The G18V CRYGS mutation associated with human cataracts increases γS-crystallin sensitivity to thermal and chemical stress, Biochemistry 48 (2009) 7334–7341.
[46] I.A. Mills, S.L. Flaugh, M.S. Kosinski-Collins, J.A. King, Folding and stability of the isolated Greek key domains of the long-lived human lens proteins γD-crystallin and γS-crystallin, Protein Sci. 16 (2007) 2427–2444.
[47] J.J. Harding, Disulphide cross-linked protein of high molecular weight in human cataractous lens, Exp. Eye Res. 17 (1973) 377–383.
[48] S. Najmudin, V. Nalini, H.P.C. Driessen, C. Slingsby, T.L. Blundell, D.S. Moss, P.F. Lindley, Structure of the bovine eye lens protein γB(γII)-crystallin at 1.47 Å, Acta Crystallogr. D 49 (1993) 223–233.
[49] R.J. Siezen, J.A. Thomson, E.D. Kaplan, G.B. Benedek, Human lens gamma-crystallins: isolation, identification, and characterization of the expressed gene products, Proc. Natl. Acad. Sci. U. S. A. 84 (1987) 6088–6092.
[50] V.M. Berthoud, E.C. Beyer, Oxidative stress, lens gap junctions, and cataracts, Antioxid. Redox Signal. 11 (2009) 339–353.
[51] M.H. Garner, A. Spector, Selective oxidation of cysteine and methionine in normal and senile cataractous lenses, Proc. Natl. Acad. Sci. U. S. A. 77 (1980) 1274–1277.
[52] J.N. Liang, M.R. Pelletier, Spectroscopic studies on the mixed disulfide formation of lens crystallin with glutathione, Exp. Eye Res. 45 (1987) 197–206.
[53] M.F. Lou, J.E. Dickerson, Protein-thiol mixed disulfides in human lens, Exp. Eye Res. 55 (1992) 889–896.
[54] C. Slingsby, L. Miller, The reaction of glutathione with the eye-lens protein γ-crystallin, Biochem. J. 230 (1985) 143–150.
[55] W.D. Brubaker, J.A. Freites, K.J. Golchert, R.A. Shapiro, V. Morikis, Douglas J. Tobias, R.W. Martin, Separating instability from aggregation propensity in γS-crystallin variants, Biophys. J. 100 (2011) 498–506.
[56] J.M. Hemmingsen, K.M. Gernert, J.S. Richardson, D.C. Richardson, The tyrosine corner: a feature of most Greek key β-barrel proteins, Protein Sci. 3 (1994) 1927–1937.
[57] S. Bagby, S. Go, S. Inouye, M. Ikura, A. Chakrabartty, Equilibrium folding intermediates of a Greek key β-barrel protein, J. Mol. Biol. 276 (1998) 669–681.
[58] S. Lee, B. Mahler, J. Toward, B. Jones, K. Wyatt, L. Dong, G. Wistow, Z. Wu, A single destabilizing mutation (F9S) promotes concerted unfolding of an entire globular domain in γS-crystallin, J. Mol. Biol. 399 (2010) 320–330.
[59] E. Serebryany, J.A. King, The βγ-crystallins: native state stability and pathways to aggregation, Prog. Biophys. Mol. Biol. 115 (2014) 32–41.
[60] M.J. Whitley, Z. Xi, J.C. Bartko, M.R. Jensen, M. Blackledge, A.M. Gronenborn, A combined NMR and SAXS analysis of the partially folded cataract-associated V75D γD-crystallin, Biophys. J. 112 (2017) 1135–1146.
[61] P. Das, J.A. King, R. Zhou, Aggregation of γ-crystallins associated with human cataracts via domain swapping at the C-terminal β-strands, Proc. Natl. Acad. Sci. U. S. A. 108 (2011) 10514–10519.
[62] J.C. Boatz, M.J. Whitley, M. Li, A.M. Gronenborn, P.C.A. van der Wel, Cataract-associated P23T γD-crystallin retains a native-like fold in amorphous-looking aggregates formed at physiological pH, Nat. Commun. 8 (2017), 15137.
[63] W. Kabsch, XDS, Acta Crystallogr. D Biol. Crystallogr. 66 (2010) 125–132.
[64] A.J. McCoy, R.W. Grosse-Kunstleve, P.D. Adams, M.D. Winn, L.C. Storoni, R.J. Read, Phaser crystallographic software, J. Appl. Crystallogr. 40 (2007) 658–674.
[65] P.D. Adams, P.V. Afonine, G. Bunkóczi, V.B. Chen, I.W. Davis, N. Echols, J.J. Headd, L.-W. Hung, G.J. Kapral, R. W. Grosse-Kunstleve, PHENIX: a comprehensive Python-based system for macromolecular structure solution, Acta Crystallogr. D Biol. Crystallogr. 66 (2010) 213–221.
[66] P. Emsley, K. Cowtan, Coot: model-building tools for molecular graphics, Acta Crystallogr. D Biol. Crystallogr. 60 (2004) 2126–2132.
[67] P.V. Konarev, V.V. Volkov, A.V. Sokolova, M.H. Koch, D.I. Svergun, PRIMUS: a Windows PC-based system for small-angle scattering data analysis, J. Appl. Crystallogr. 36 (2003) 1277–1282.
[68] D. Svergun, Determination of the regularization parameter in indirect-transform methods using perceptual criteria, J. Appl. Crystallogr. 25 (1992) 495–503.
[69] D. Svergun, C. Barberato, M.H. Koch, CRYSOL—a program to evaluate X-ray solution scattering of biological macromolecules from atomic coordinates, J. Appl. Crystallogr. 28 (1995) 768–773.
[70] D.I. Svergun, M.V. Petoukhov, M.H. Koch, Determination of domain structure of proteins from X-ray solution scattering, Biophys. J. 80 (2001) 2946–2953.
[71] V.V. Volkov, D.I. Svergun, Uniqueness of ab initio shape determination in small-angle scattering, J. Appl. Crystallogr. 36 (2003) 860–864.
[72] D.I. Svergun, Restoring low resolution structure of biological macromolecules from solution scattering using simulated annealing, Biophys. J. 76 (1999) 2879–2886.
[73] E.F. Pettersen, T.D. Goddard, C.C. Huang, G.S. Couch, D.M. Greenblatt, E.C. Meng, T.E. Ferrin, UCSF Chimera—a visualization system for exploratory research and analysis, J. Comput. Chem. 25 (2004) 1605–1612.
[74] F. Sievers, A. Wilm, D. Dineen, T.J. Gibson, K. Karplus, W. Li, R. Lopez, H. McWilliam, M. Remmert, J. Söding, Fast,

scalable generation of high-quality protein multiple sequence alignments using Clustal Omega, Mol. Syst. Biol. 7 (2011) 539.
[75] D. Cox, E. Selig, M.D. Griffin, J.A. Carver, H. Ecroyd, Small heat shock proteins prevent α-synuclein aggregation via transient interactions and their efficacy is affected by the rate of aggregation, J. Biol. Chem. 291 (2016) 22618–22629.